Experimental and numerical study concerning the anisotropic behavior of an AA2024-T351 thick sheet using the unified formalism, a multi-mechanism model and a polycrystalline approach

Walid NASRI[a,b], Adinel GAVRUS[a], Afia KOUADRI-DAVID[a], Kacem SAI[b]

a. LGCGM – EA3913, INSA, UEB, 20 Av. des Buttes de Coësmes, 35708 Rennes, France.
walid.nasri@insa-rennes.fr, adinel.gavrus@insa-rennes.fr, afia.kouadri-henni@insa-rennes.fr
b. LGPMM, Ecole Nationale d'Ingénieurs de Sfax, BP. 1173 – 3038, Sfax, Tunisie.
kacemsai@yahoo.fr

Abstract:

The purpose of this work is to evaluate the anisotropic mechanical behavior of an AA2024-T351 thick plate using three multi-scales approaches: a Macroscopic Unified formalism (HILL 48), a Multi-Mechanisms Model and a Polycrystalline plasticity model. The experimental results obtained from uniaxial tensile tests are first described. Thereafter, the theoretical formulations and numerical identification of studied elastoplastic approaches are presented. Finally, finite element simulations of tensile tests and analysis of the thick sheet stretching forming process are performed.

Keywords: **Thick sheet anisotropy, Multi-scale modelling, Numerical simulation, Aluminium alloy, Stretching forming.**

1   Introduction

In the aeronautical manufacturing industry, due to the important need for low-weight, aircraft elements made in aluminium alloy characterized by good mechanical resistance and formability are used. Generally this material is obtained in a sheet or plate form by hot and cold rolling forming processes which creates plastic anisotropy. This phenomenon is the result of the distortion of the plastic yield surface shape due to the material microstructural state change [1]. It is important to understand the anisotropic mechanical behavior characterizing a thin [2] or a thick sheet and ensure the reliability of the numerical models prediction in order to be integrated in general engineering optimal design analysis or to be strongly used for improvements of sheet forming processes. This work presents an introduction of the three-dimensional anisotropy study of an aluminium alloy and starts with two specific cases of a 3D plastic anisotropy: normal and planar. In normal anisotropy (used for studying thin and thick sheets), the properties differ principally in the thickness direction. Whereas, in planar anisotropy (used classically for studying thin sheets), the properties vary with the orientation in the plane of the sheet. Three different elasto-plastic numerical approaches are in the focus of this proposed study: a unified formalism, a multi-mechanism model and a polycrystalline one [3-7]. To demonstrate their feasibility and to select the most accurate model describing the plastic anisotropy, comparisons are realized with the experimental data obtained from tensile tests performed for specimens with a thickness of 3 mm along different directions to the rolling direction. Finite Element analyses based on

the three numerical models are used for the simulation of uni-axial tensile tests and of a stretching forming process in order to evaluate their robustness on analysis of severe material forming conditions.

2   Experimental study

2.1   The sample material and operating conditions

Uni-axial tensile tests were carried out on flat pieces of smooth sections obtained by machining from a rolled AA2024-T351 thick plate. The loading axis of specimens with a thickness of 3 mm coincides with different cutting directions with respect to the rolling direction. Figure 1 shows the used specimen's geometrical dimensions.
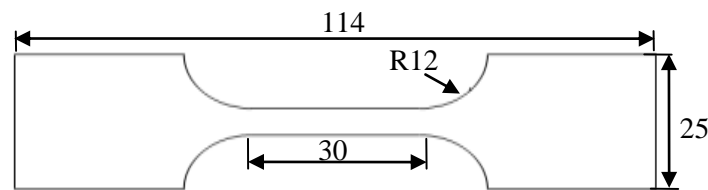
Figure 1: Plane specimen dimensions (*in mm*)

The experimental tensile tests were conducted in the directions 0°, 30°, 45°, 60°, 75° and 90° with respect to the rolling direction using an INSTRON machine of INSA Rennes having a maximum loading capacity of 50 kN (figure 2), recording both the loads and the displacements controlling a constant crosshead speed of 5 mm/min corresponding to an initial strain rate of $\dot{\varepsilon}=2 \times 10^{-3} s^{-1}$.
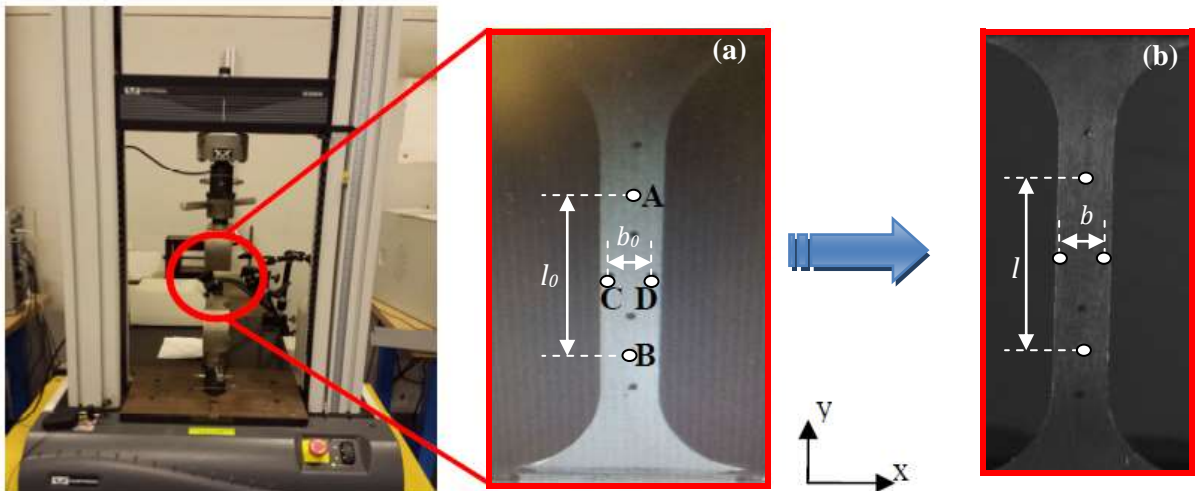
Figure 2: INSTRON universal testing machine and the tasks points (A, B, C, D) positioned on the tensile specimen surface: **(a)** before and **(b)** after the test.

2.2   Experimental results and classical analysis

Axial load and displacements in longitudinal and transverse directions was recorded during the experiment using a speed camera measuring respectively two point's displacements throughout the material traction (figure 2). Then the camera follows two points A and B along the y axis of loading (having an initial distance l_0 between them) and two points C and D along the x axis (spaced by an initial distance b_0).

Thanks to the digital images of the specimen, the evolution of each local distance can be recorded and then to estimate the corresponding total strains ε_{yy}^t, ε_{xx}^t using the following formula:

$$\varepsilon_{yy}^t = ln\left(\frac{l}{l_0}\right) \text{ and } \varepsilon_{xx}^t = ln\left(\frac{b}{b_0}\right) \tag{1}$$

l, b are the measured displacements.

The tensile load F was continuously measured in order to evaluate the true stress:

$$\sigma_{yy} = \frac{F}{S_0} exp\left(\varepsilon_{yy}^t\right) \tag{2}$$

S_0 is the cross section area of the specimen.

The corresponding plastic strain is obtained from the partition of the total strain by an elastic part and a plastic one:

$$\dot{\varepsilon}^t = \dot{\varepsilon}^e + \dot{\varepsilon}^p \text{ or } d\varepsilon^t = d\varepsilon^e + d\varepsilon^p \tag{3}$$

According to the three orthotropic axes (*x,y,z*) the plastic strains can then be calculated as follows:

$$\varepsilon_{xx}^p = \varepsilon_{xx}^t + \frac{\upsilon\sigma_{yy}}{E} \text{ and } \varepsilon_{yy}^p = \varepsilon_{yy}^t - \frac{\sigma_{yy}}{E} \tag{4}$$

Using the volume conservation principle ($tr(\dot{\tilde{\varepsilon}}^p) = 0$), the plastic strain along the specimen thickness ε_{zz}^p can be estimated by:

$$\varepsilon_{zz}^p \approx -\left(\varepsilon_{xx}^p + \varepsilon_{yy}^p\right) \tag{5}$$

Starting from the classical plastic anisotropy theory of a thin sheet, the Lankford coefficient, denoted *r*-value, was estimated from different tensile directions with respect to the rolling one (0°, 45° and 90˚), using the ratio between the plastic width strain ε_{xx}^p and the thickness strain ε_{zz}^p [8]:

$$r = \frac{\dot{\varepsilon}_{xx}^p}{\dot{\varepsilon}_{zz}^p} = \frac{d\varepsilon_{xx}^p}{d\varepsilon_{zz}^p} \approx \frac{\varepsilon_{xx}^p}{\varepsilon_{zz}^p} \tag{6}$$

It is shown that the *r*-value is equal to one for isotropic materials and any other value indicates that plastic anisotropy occurs during the material deformation. The normal anisotropy $\bar{r}$ and the planar anisotropy $\varDelta r$ are also used to investigate the formability and the earring pattern in circular cup drawing. Higher value of $\bar{r}$ means a less thinning and a better formability. On the other hand, higher planar anisotropy $\varDelta r$ means more anisotropic properties. The two parameters can be computed as:

$$\bar{r} = \frac{r_0 + 2r_{45} + r_{90}}{4} \text{ and } \varDelta r = \frac{r_0 - 2r_{45} + r_{90}}{2} \tag{7}$$

Here the r_0, r_{45}, r_{90} are the Lankford coefficients estimated by equation (6). For the 0°, 45° and 90° tensile tests, the obtained experimental true stress-true strain curves before the onset of the specimen necking are shown in the figure 3 (**a**). As it can be seen, a close material behavior is obtained between the tensile directions 45° (DD) and 90° (TD). The plastic behavior of the specimen loaded at 0° (RD) is slightly different in intensity with a dozen of MPa. Some differences can be observed in the figure 3 (**b**) comparing to a thin AA2024 sheet [2]. Because the planar anisotropy $\varDelta r$ has smaller values (i.e.

Δr = -0.07 for 10% plastic deformation), it is possible to consider that the considered AA2024 thick plate has rather a normal anisotropy, which is a particular case of a 3D anisotropy. Moreover an average Lankford coefficient lowers than 1 ($\bar{r}$ =0.64 for 10% plastic deformation) reflects a less good formability of this material.
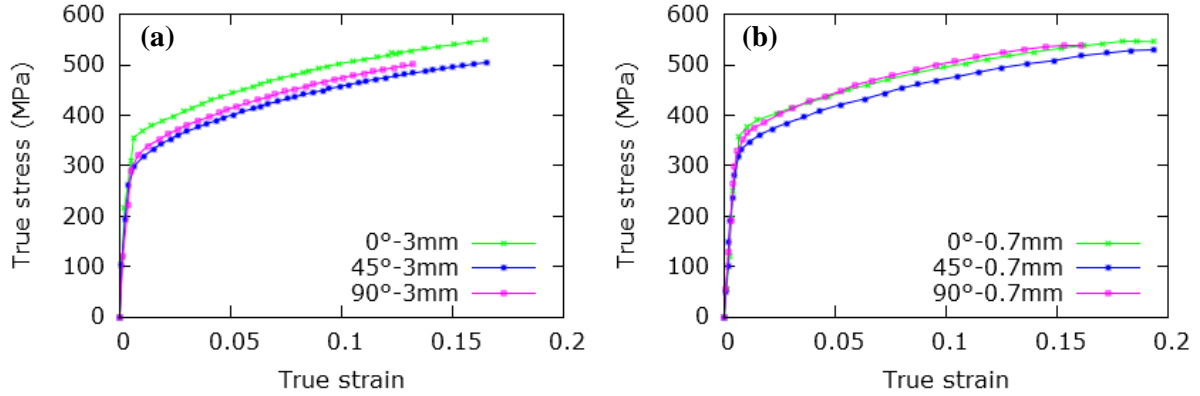

Figure 3: Experimental true stress–true strain curves along the tensile directions 0°, 45° and 90° of AA2024-T351: **(a)** thick plate (present work) and **(b)** thin sheet [2]

If a Hill's 1948 quadratic plastic anisotropic behaviour law is taking into account, the variations of the corresponding coefficients with the plastic strain (F', G', H', L', M', N' or dimensionless F, G, H, L, M, N ones) seems to be in accordance with the classical analysis of the plane anisotropy (equation (9)) and normal anisotropy (equation (10)). These coefficients can be expressed in function of Lankford parameters using the following expressions:

$$\begin{cases} F = \dfrac{r_0}{r_{90}(1+r_0)} \; ; F' = \dfrac{F}{\sigma_0^2} \\[2mm] G = \dfrac{1}{(1+r_0)} \; ; G' = \dfrac{G}{\sigma_0^2} \\[2mm] H = \dfrac{r_0}{(1+r_0)} \; ; H' = \dfrac{H}{\sigma_0^2} \\[2mm] N = \dfrac{(r_0+r_{90})(1+2r_{45})}{2r_{90}(1+r_0)} \; ; N' = \dfrac{N}{\sigma_0^2} \end{cases} \quad (9) \qquad \begin{cases} F = G = \dfrac{1}{(1+\bar{r})} \; ; F' = G' = \dfrac{1}{\sigma_0^2(1+\bar{r})} \\[2mm] H = \dfrac{\bar{r}}{(1+\bar{r})} \; ; H' = \dfrac{\bar{r}}{\sigma_0^2(1+\bar{r})} \\[2mm] N = F+2H \; ; N' = F'+2H' \end{cases} \quad (10)$$

where σ_0 is the equivalent stress corresponding to the tensile behavior along the rolling direction DL.

The evolution of these coefficients with the cumulated plastic strain is plotted in figures 4. In a first approximation, estimating all the r coefficients for 0.2% of plastic deformation, the dimensionless Hill coefficients F, G, H and N have constant values.
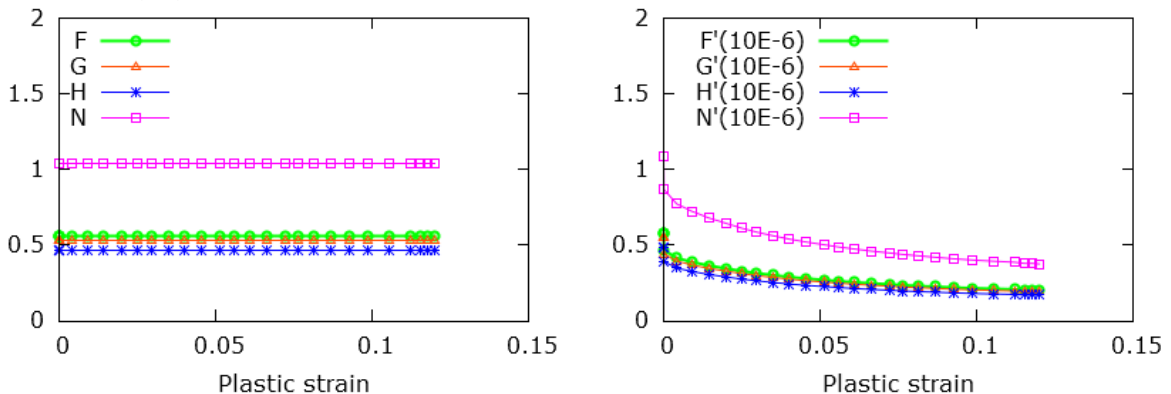

Figure 4: Variations of the computed Hill coefficients as a function of the plastic strain for a plane anisotropy

The variations of the Hill coefficients (F', G', H', N') exhibit a sharp fall before a plastic strain of 5%. Beyond this level, these coefficients decrease slowly. Commonly, constant values of the Hill coefficients computed for a 0.2% plastic strain are generally used in the phenomenological anisotropic models. Nonetheless this assumption, to gives a more accurate Hill's 1948 criterion describing the plastic anisotropy of aluminum alloys, the anisotropy coefficients must be estimated for each plastic deformation degree and consequently variations of these coefficients with the plastic strain will be analyzed starting from obtained experimental data. The evolution of the three Lankford coefficients (r_0, r_{45} and r_{90}) corresponding to the plane anisotropy and of the average Lankford coefficient $\bar{r}$ corresponding to the normal anisotropy are plotted respectively in figure 5 and figure 6 together with a polynomial interpolation equation characterizing quantitatively their variations.
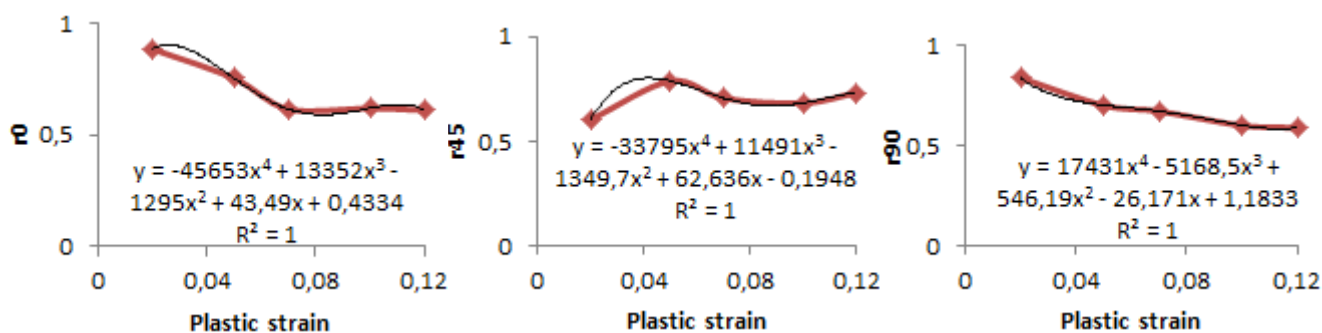
Figure 5: Four degree polynomial interpolation of r_0, r_{45} and r_{90} Lankford coefficients according to their variation with the plastic strain
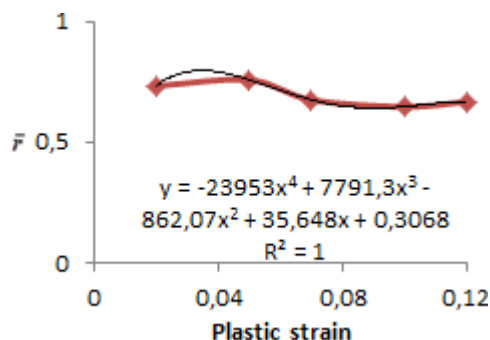
Figure 6: Four degree polynomial interpolation of normal anisotropy coefficient $\bar{r}$ according to its variation with the plastic strain

The corresponding curves representing the variation of the Hill coefficients computed from equations (9) and (10) are plotted in figure 7 for the normal anisotropy and in figure 8 for the plane anisotropy.
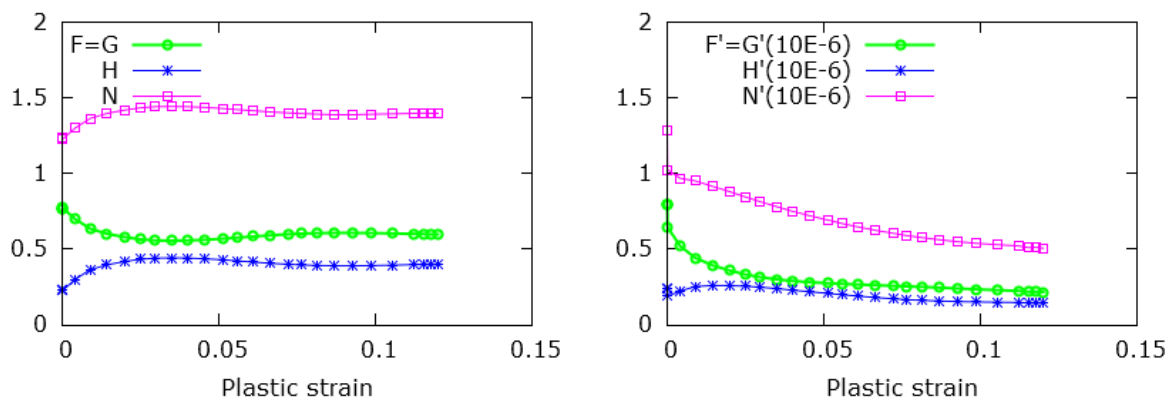
Figure 7: Variations of the computed Hill coefficients as a function of the plastic strain for a normal anisotropy
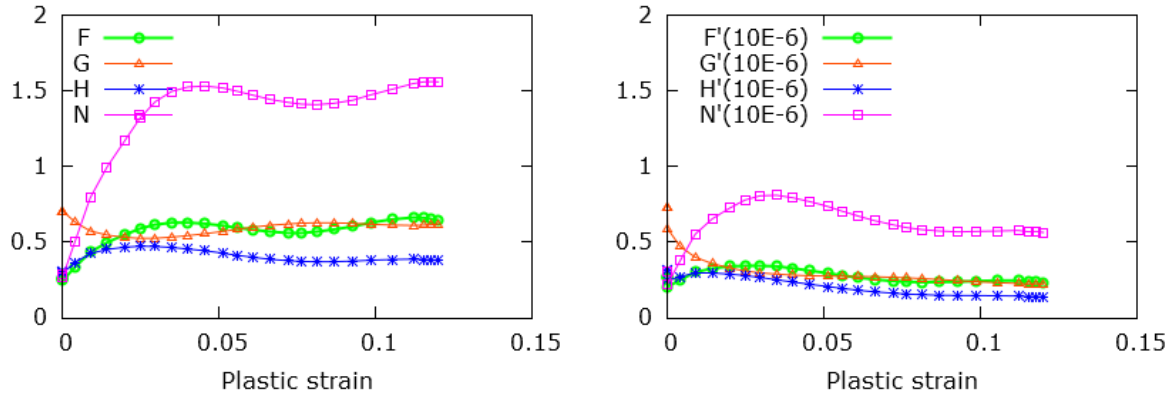
Figure 8: Variations of the computed Hill coefficients as a function of the plastic strain for a plane anisotropy

It can be observed that during the material plastic deformation the Hill coefficients have significance variations with respect to the plastic strain. Then, as compared to the estimated values for 0.2% or 2% of plastic deformation, the coefficients have different values for 5%, 7% or 10% of plastic strain. Consequently this observed variation must be taking into account by more realistic numerical simulations of forming processes as the stretching, deep drawing and stamping.

3   The constitutive equations

Dealing with the elasto-plastic behavior of aluminum alloys dedicated to metal forming it is convenient to use a finite strain formulation by the mean of an updated Lagrangian formalism already implemented in the FE software ZeBuLoN [9]. The material behavior description is based on constitutive equations using tensorial internal variables and on the Green–Naghdi transformation of the stress–strain problem into an "equivalent material referential". This standard computation allows the decomposition of the incremental total strain into elastic and inelastic parts i.e. $d\varepsilon^t = d\varepsilon^e + d\varepsilon^p$.

The numerical strategy generally used to take into account a 3D plastic anisotropy in a classical Macroscopic Unified model (Table 1) is to involve a tensor of fourth order into the criterion expression. [3, 4, 7].

Table 1: Constitutive Equations of the Unified Model

$f(\tilde{\sigma}) = \sqrt{\dfrac{3}{2}(\tilde{s} - \tilde{X}):\tilde{\tilde{B}}:(\tilde{s} - \tilde{X})} - R$ $\tilde{X} = (2/3)C\tilde{\alpha}$; $R = R_0 + Q[1-exp(-b\lambda)]$ $\dot{\tilde{\varepsilon}}^p = \dot{\lambda}\dfrac{\partial f}{\partial \tilde{\sigma}} = \dot{\lambda}\tilde{n}$; $\dot{\tilde{\alpha}} = \dot{\lambda}(\tilde{n} - D\tilde{\alpha})$ $f(\tilde{\sigma}) = \sqrt{\begin{array}{l}F(\sigma_{yy} - \sigma_{zz})^2 + G(\sigma_{zz} - \sigma_{xx})^2 \\ + H(\sigma_{xx} - \sigma_{yy})^2 + 2L\sigma_{yz}^2 + 2M\sigma_{xz}^2 + 2N\sigma_{xy}^2\end{array}} - R$	• $\tilde{\tilde{B}}$: Fourth order tensor • $\tilde{X}$: Back stress variable • $\tilde{\alpha}$: Hardening variable • R :Size of elastic domain • R_0 : Initial size of R • Q, b, C, D: Material parameters • $\dot{\lambda}$: Plastic multiplier • λ : Represents equivalent plastic strain. • (F, G, H, L, M, N): Hill coefficients

To take into account physical plastic phenomena at a mesoscopic scale, a multi-mechanisms model has been developed. In this case the inelastic strain rate $\dot{\tilde{\varepsilon}}^p$ is split into two components: $\dot{\tilde{\varepsilon}}^p = \dot{\tilde{\varepsilon}}^1 + \dot{\tilde{\varepsilon}}^2$ where $\dot{\tilde{\varepsilon}}^1$ and $\dot{\tilde{\varepsilon}}^2$ are the local inelastic strain rate of the mechanism 1 and 2 respectively. Table 2 summarizes the constitutive equations of the named 2M1C model (2 mechanisms, 1 criterion).

Table 2: Multi-Mechanisms models (2M1C)

$\dot{\tilde{\varepsilon}}^p = \dot{\tilde{\varepsilon}}^1 + \dot{\tilde{\varepsilon}}^2$ $f = \sqrt{\left(J_L(\tilde{\sigma} - \tilde{X}^1) \right)^2 + \left(J_L(\tilde{\sigma} - \tilde{X}^2) \right)^2} - R$ $J_{LI} = J_L(\tilde{\sigma} - \tilde{X}^1) = \sqrt{\frac{3}{2}(\tilde{s} - \tilde{X}^1) : \tilde{\tilde{L}} : (\tilde{s} - \tilde{X}^1)} \; ; I=1,2$ $R = R_0 + Q[1 - exp(-b\lambda)]$ $\begin{pmatrix} \tilde{X}^1 \\ \tilde{X}^2 \end{pmatrix} = \frac{2}{3}\begin{pmatrix} C_{11} & C_{12} \\ C_{12} & C_{22} \end{pmatrix}\begin{pmatrix} \tilde{\alpha}^1 \\ \tilde{\alpha}^2 \end{pmatrix}; \; \tilde{n}^1 = \frac{3}{2}\frac{\tilde{\tilde{L}}:(\tilde{s} - \tilde{X}^1)}{(J_{LI}^2 + J_{LI}^2)^{1/2}}$ $\dot{\tilde{\alpha}}^1 = \dot{\lambda}(\tilde{n}^1 - \frac{3}{2}\frac{D_1}{C_{11}}\tilde{X}^1) \; ; \dot{\tilde{\alpha}}^2 = \dot{\lambda}(\tilde{n}^2 - \frac{3}{2}\frac{D_2}{C_{22}}\tilde{X}^2)$	• f : Yield criterion function • $\dot{\tilde{\varepsilon}}^p$: Tensor of plastic strain rate • $\dot{\tilde{\varepsilon}}^1$: Tensor of local inelastic strains rate of the mechanism I • $\tilde{X}^1$: Back stress tensor of each mechanism I • $\tilde{\tilde{L}}$: Fourth order tensor • $C_{11}, C_{12}, C_{22}, D_1, D_2$: Kinematic hardening moduli • $\tilde{n}^1$: Normal to the yield surface for each mechanism • $\tilde{\alpha}^1$: Kinematic internal variables

For a multi-scale approach taking into account the plasticity as a microstructural scale, the polycrystalline plasticity model seems to be the most appropriate. In this case the plastic deformation is the result of the dislocations glides along the active directions of crystallographic systems defining the metallic crystal structure (FCC for AA2024).
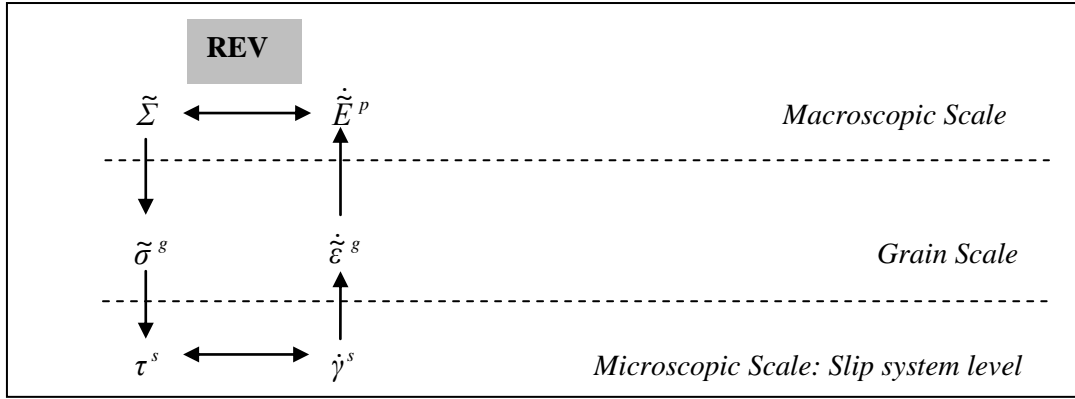

Figure 9: Diagram of the Polycrystalline model using REV method

Table 3: Equations of the Polycrystalline model

$\tilde{\sigma}^g = \tilde{\Sigma} + C(\langle \tilde{\beta}^g \rangle - \tilde{\beta}^g); \; \dot{\tilde{\beta}}^g = \dot{\tilde{\varepsilon}}^g - D\tilde{\beta}^g \|\dot{\tilde{\varepsilon}}^g\|$ $\tau^s = \tilde{\sigma}^g : \tilde{m}_s^g \; with \; \tilde{m}_s^g = \frac{1}{2}[\tilde{n}^s \otimes l^s + l^s \otimes \tilde{n}^s]$ $\dot{\gamma}_s = \left\langle \frac{|\tau^s - x^s| - r^s}{k} \right\rangle^n sign(\tau^s - x^s)$ $\dot{x}^s = c\dot{\gamma}^s - \dot{v}^s d x^s$ $r^s = r_0 + Q\sum H^{rs}(1 - bv^r) \; with \; \dot{v}^r = |\dot{\gamma}^r|$ $\dot{\tilde{\varepsilon}}^g = \sum_{s=1}^{12} \tilde{m}_s^g \dot{\gamma}_s$ $\dot{\tilde{E}}^p = \langle \dot{\tilde{\varepsilon}}^g \rangle$	• $\dot{\tilde{E}}^p$: Macro plastic strain rate • $\tilde{\Sigma}$: Macro stress • $\tilde{\sigma}^g$: Local grain stress • $\tilde{\beta}^g$: Hardening variable for each grain • C and D: Material parameters • τ^s : Local shear stress • $\tilde{m}_s^g$: Orientation tensor • $\dot{\gamma}_s$: Shear rate • k and n : Material coefficients • r^s : Variable of isotropic hardening • x^s : Variable of kinematic hardening • r_0 : Initial critical shear stress • b: Rate of saturation • c and d : Material parameters • Q : Hardening capacity • H^{rs}: Hardening matrix

In a numerical point of view the polycrystalline model uses the concept of a representative elementary volume (REV) which can be coupled to a finite element method. Figure 9 shows a simplified diagram of the Polycrystalline model approach detailed in Ref. [5] and adopted in this work (Table 3).

All the three above material constitutive models: the macroscopic unified, the multi-mechanisms (MM − 2M1C) and the polycrystalline plasticity one are implemented into the material library ZMaT and the subroutine ZSeT of the finite element code ZeBuLoN [9] using a θ-method solver via an implicit Newton scheme applied for the local integration.

4   Finite element modeling and parameter identification

Finite element simulations of each presented models requires a well known of constitutive parameters values. These ones can be carried in two stages. Firstly an initial estimation of the parameters values are obtained via an interactive-graphic method based on manual comparisons between the experimental results and those obtained from numerical simulations. Final identified values are obtained using the optimization module of ZeBuLoN to improve the solution by an automatic non-linear regression. Figure 10 shows the principle of the numerical optimization technique used to identify the parameters of a defined behavior law or constitutive model.
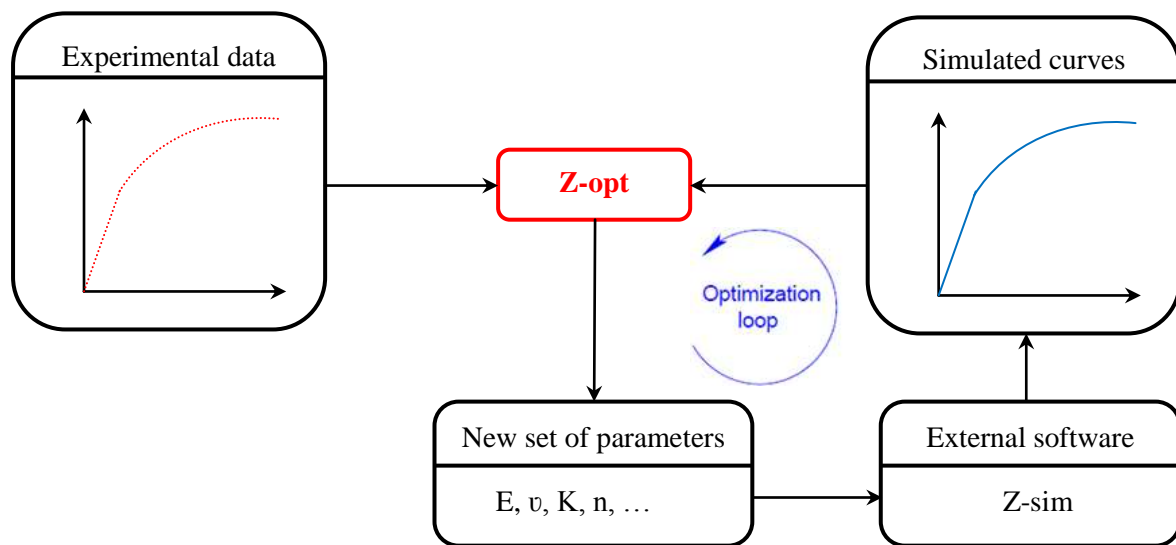

Figure 10: Optimization principle in the subroutine ZSeT

A similar tensile specimen as the experimental one is used for the numerical simulation and its finite element mesh is presented in figure 11.
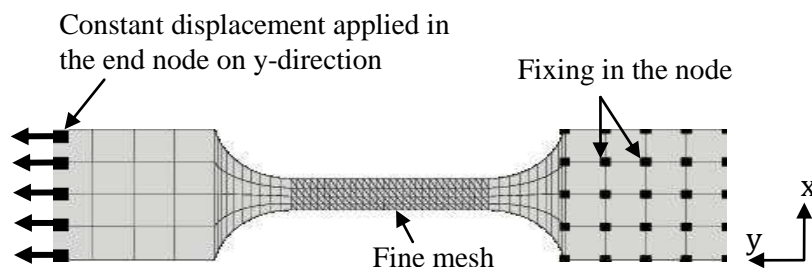

Figure 11: Finite Element meshes for the tensile specimen

Figure 12 shows a numerical simulation of a tensile test along the rolling direction using a Voce law describing an isotropic hardening (without kinematic hardening) identified from the experimental tensile test at 0° and defined by: $R = 301 + 250[1 - exp(-18\lambda)]$.
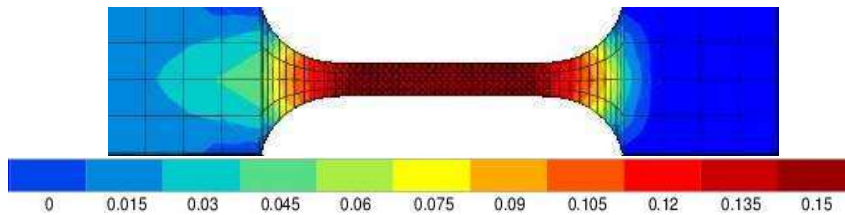

Figure 12: Numerical simulation of the tensile test

It can be observed that a homogeneous state of strains occurs in the active area of the tensile specimens which confirms the hypothesis of the homogeneity used by the classical computation's methods to estimate all variables describing the uni-axial test, the mechanical behavior and especially the anisotropy.

Macroscopic Unified Model

In the case of the macroscopic unified model, the identification results of all the parameters are presented in table 4, using a lot of FE simulations. Even if variations of Hill coefficients are not taken into account it is obtained a good agreement between the experiment and simulation of a simple tensile test (Figure 13).
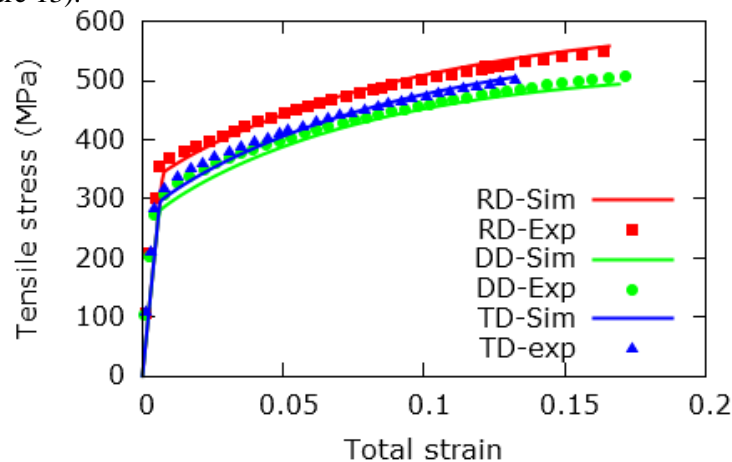

Figure 13: Comparisons between experimental and simulated tensile tests for the macroscopic unified model without kinematic hardening

Table 4: Identified parameters of the anisotropic unified model without kinematic hardening (MPa)

Elasticity		Isotropic hardening			Kinematic hardening	
E	*υ*	*R₀*	*Q*	*b*	*C*	*D*
80000	0.33	301	250	18	0	0

Hill's 48 parameters

Plane anisotropy					
F	*G*	*H*	*L*	*M*	*N*
0.5	0.63	0.37	0.97	0.97	0.97
Normal anisotropy					
F	*G*	*H*	*L*	*M*	*N*
0.63	0.63	0.36	1.35	1.35	1.35

Multi-Mechanisms Model (2M1C)

For the multi-mechanisms model (2M1C) the identified anisotropic material parameters are shown in table 5 (*the isotropic parameters L_e and L_f are not identified here*). The numerical simulation are in very good agreement with the experiments and more accurate than the results given by the previous unified model. The comparisons between the stress-strain curves simulation and experimental data were illustrated by figure 14.
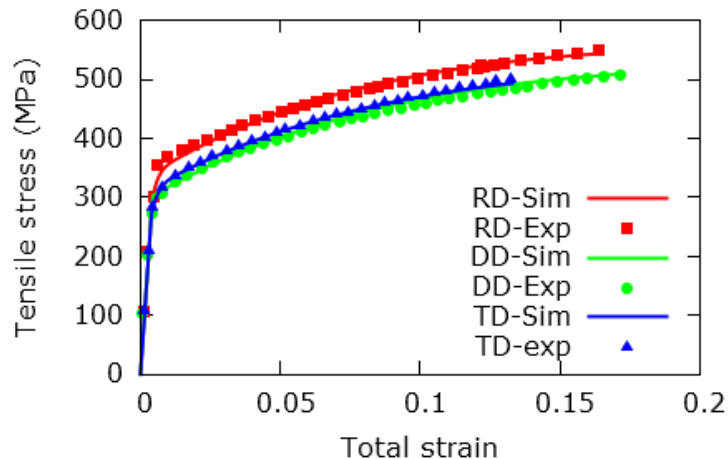

Figure 14: Comparisons between experimental and simulated tensile tests for the Multi-Mechanisms (2M1C) model

Table 5: Identified parameters of the anisotropic 2M1C model

E	v	R_0	Q	C_{11}	C_{22}	C_{12}
80000	0.33	360	260	1200	2500	900
b	D_1	D_2	L_a	L_b	L_c	L_d
7	5	5	1	1	0.2	0.5

Polycrystalline Model

For the polycrystalline model of an aluminum alloy, the crystallographic texture reported in this study is taken from the literature and has been also used to characterize the AA2024 material. An initial {111} pole figure approximated by a set of 212 orientations corresponding to an initial material state and constructed using a numerical stereographic projection code (*Projstern*) is shown in figure 15 **(a)**. The identified parameters values obtained from the best fit between the experimental data and those obtained from FE simulations (figure 15 **(b)**) are given in Table 6.
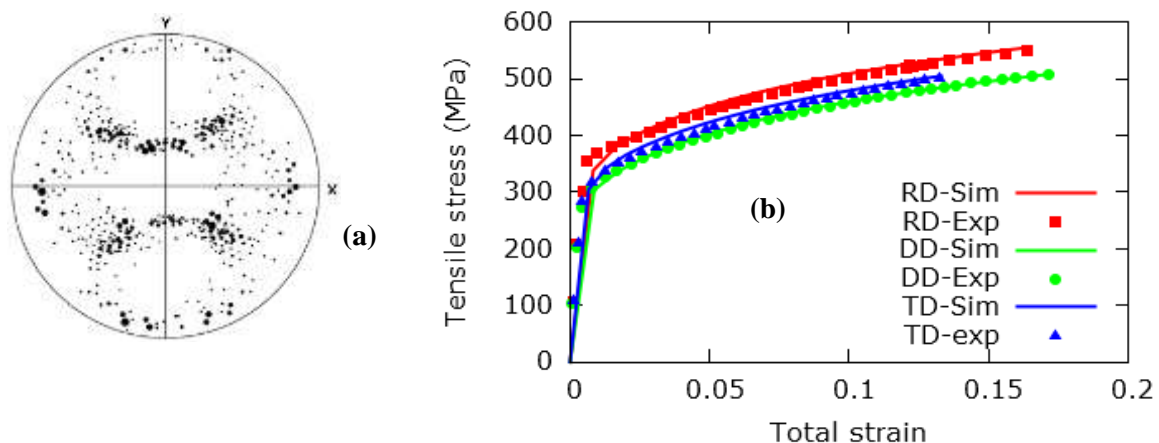

Figure 15: **(a)** {111} Pole figure and **(b)** comparisons between experimental and simulated tensile curves for the polycrystalline model.

Table 6: Identified parameters of the polycrystalline model (MPa).

Elasticity		Isotropic hardening			Norton parameters		Kinematic hardening			
E	v	r_0	Q	b	k	n	C	D	c	d
75000	0.33	145	47	5	31	11	35000	120	4300	45

5   Application to a thick sheet stretching forming process

In the present investigation, and due to the friction between the blank holder/blank which adds an additional parameter during the numerical simulations of the deep drawing of a thick sheet, the study is limited to a stretch forming process. The stretching forming is a metal forming process in which a piece of sheet metal is stretched over a die in order to form large contoured parts and to reach the plastic area so that the elongation keeps permanent. Figure 16 shows the principle of the deep drawing process and of the corresponding device.
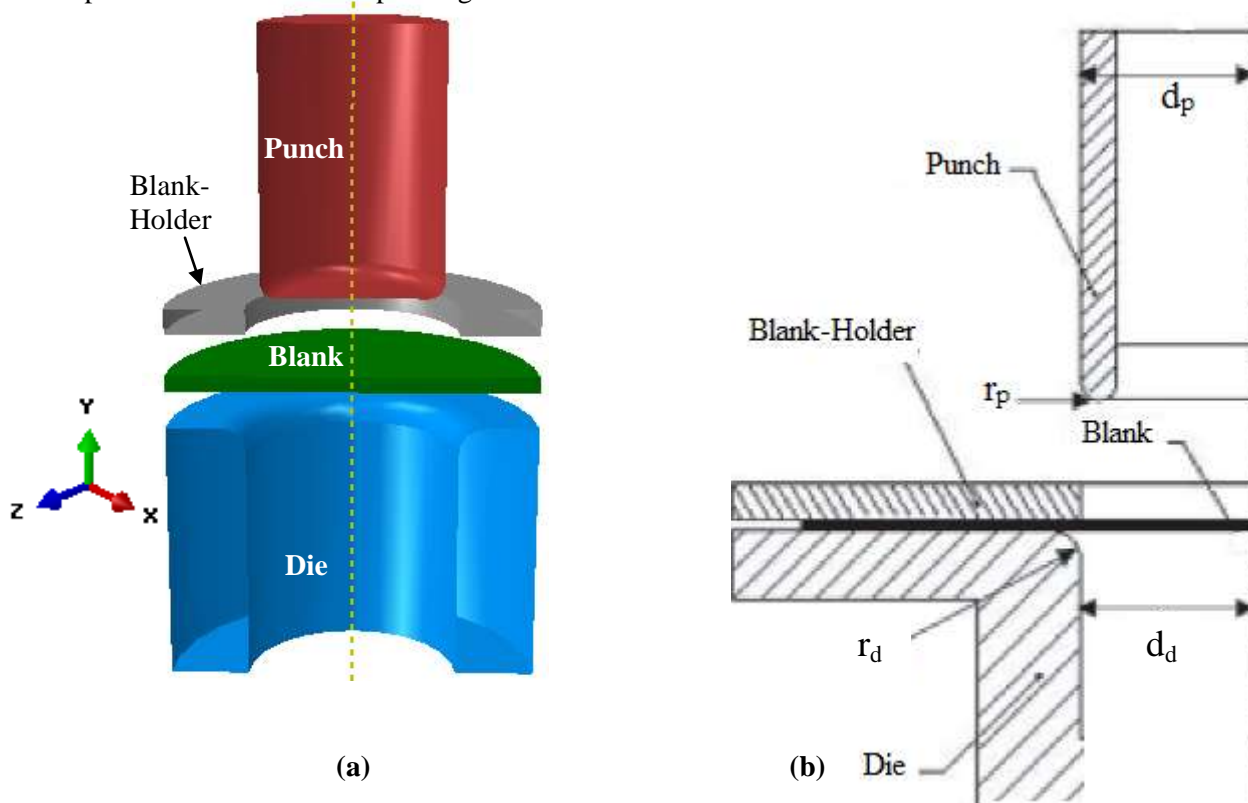

Figure 16: **(a)** 3D illustration of the deep drawing process and **(b)** The geometry of the deep drawing device.

Concerning the stretching forming this process is performed on a stretch press, in which a piece of sheet metal is securely gripped along its edges by gripping jaws. The table 7 gives the characteristic dimensions of the stretching forming device. The main advantage of the stretch forming process is the production of large parts, usually made in aluminum, with lower tooling costs as compared to the deep drawing. Generally a single pass on a single tool is required to form the sheet and mostly this process reduces the spring-back phenomenon.

The axisymmetric 2D simulation of the stretching forming operation is performed using the finite element code ZeBuLoN. The geometry of the tools and the blank is defined in figure 17. The blank, with a thickness of 3 mm, was modeled with 4-node linear axisymmetrical elements. The simulations are performed without a blank holder, considering that the sheet is placed on the die and clamped on

its edge. The stretching forming simulation was conducted under displacement control to a relative punch-displacement initially of 8 mm. The clearance between the punch and the die is 3 mm and the friction of contact between punch/blank and blank/die were defined with a coulomb model via a friction coefficient equal to 0.1.
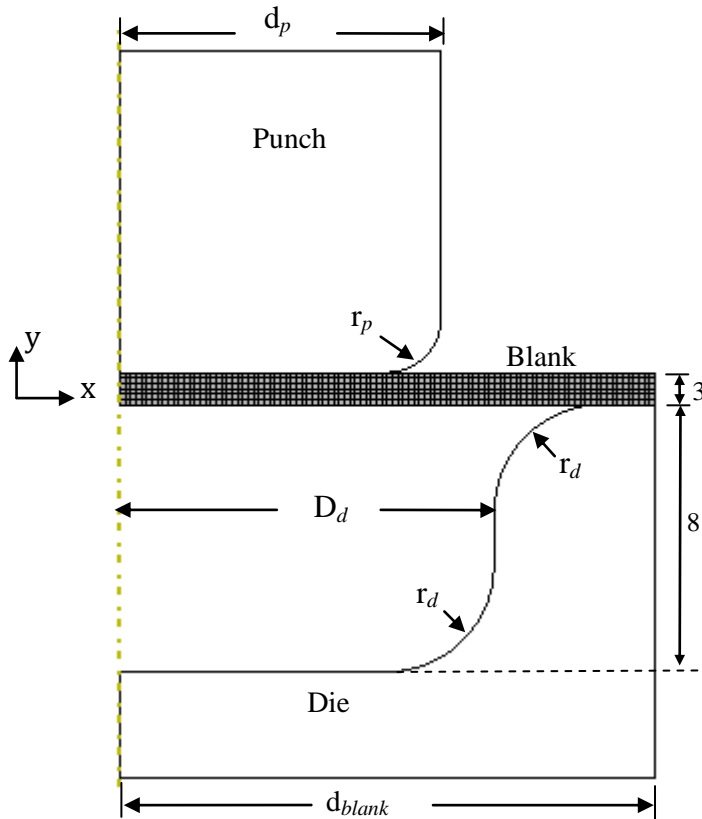

Table 7: Characteristic dimensions of the Stretching forming device (*mm*)

d_p	r_p	D_d	r_d	d_{Blank}
19.5	5	22.5	30	32.5

Figure 17: The geometry and the mesh used in a finite element stretch forming process simulation (*all dimensions in mm*)

Figure 18 shows the evolution of the numerical punch loads according to its movement during the cupping for the three presented models using numerical simulations made with ZeBuLoN code.
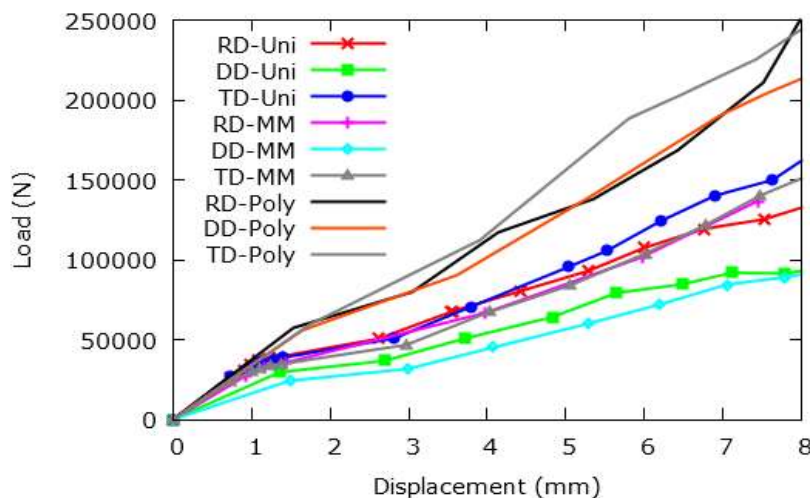

Figure 18: Numerical load-displacement curves obtained for RD, TD and DD stretching forming tests and the three models (ZeBuLoN): Macroscopic Unified, MM (2M1C) and Polycrystalline

Nearly similar shape and maximum loads are obtained for unified and 2M1C models as compared to the polycrystalline one which seems to overestimate the drawing forces.

Numerical simulations for the macroscopic unified model were performed via both Abaqus and ZeBuLoN code (Figure 19) using an isotropic hardening Voce law [10] defined by:
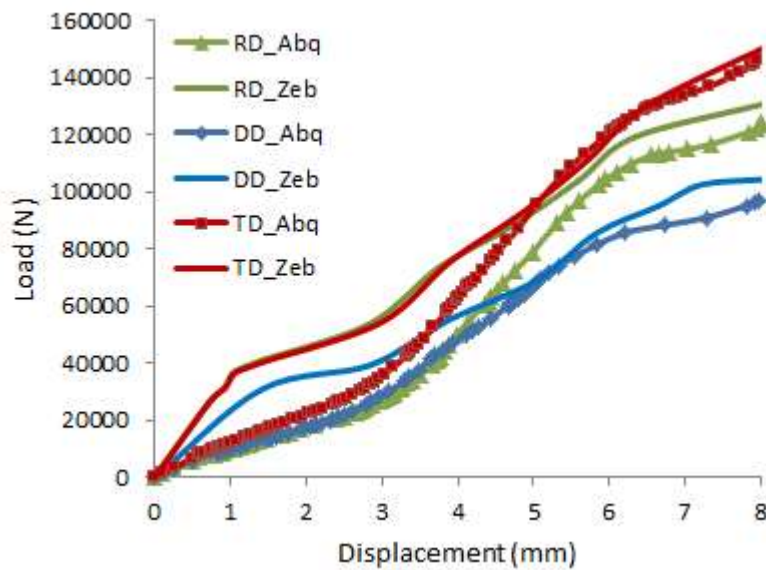$R = 301 + 250[1 - exp(-18\lambda)]$.

Figure 19: Numerical load-displacement curves obtained for RD, TD and DD drawing tests using the Macroscopic Unified model (Abaqus and ZeBuLoN).

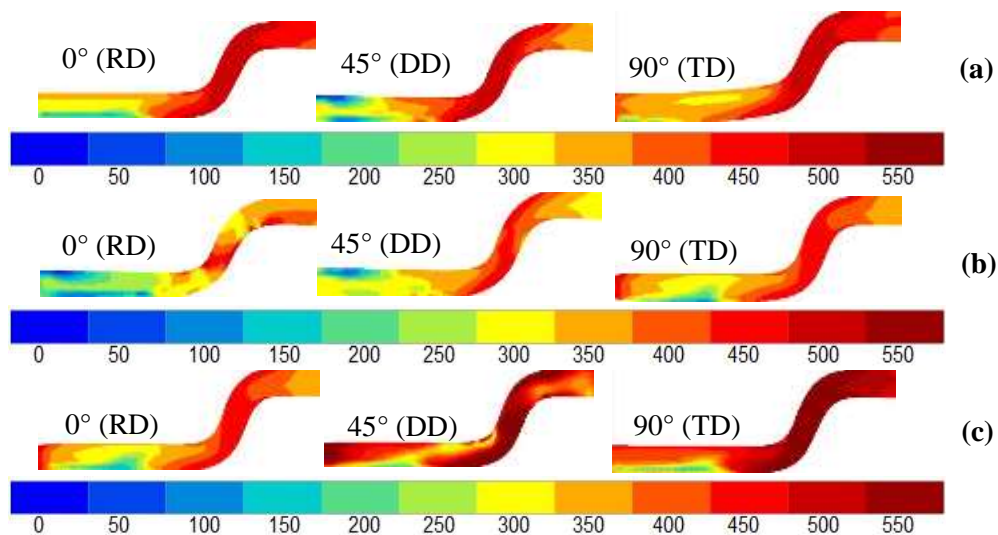The contour plots of the equivalent stress after 8 mm of punch displacement is shown in figure 20.

Figure 20: Contour plot of the equivalent stress at 8 mm depth: **(a)** Macroscopic Unified model, **(b)** MM (2M1C) model and **(c)** Polycrystalline model.

It can be observed that the macroscopic unified formalism and the 2M1C model lead to similar distribution of the equivalent stress. On the other side, the polycrystalline model gives different results principally due to the important influence of the material texture evolution. It can be concluded that for more pronounced plastic deformations the local anisotropy becomes more important that the global anisotropy taken into account by the first two models.

Conclusion

In this paper experimental analysis and three multi-scales approaches have been used to describe the plastic anisotropy for an AA2024-T351 thick sheet. Starting form the classical analysis of the plastic anisotropy has been proposed an analytical estimation of the variations of Lankford and Hill coefficients with the plastic strain. According to the three proposed constitutive models and starting from simulations of a simple tensile test, a good agreement is obtained between the numerical results and the experimental data in terms of stress-strain behavior. However it can be seen that the Multi-Mechanisms (MM) and Polycrystalline models are more accurate to simulate the anisotropy of the studied material compared to the macroscopic unified model. Finally the numerical simulations of the AA2024 thick sheet stretch forming process in different directions of the anisotropy are presented and compared for the three approaches. The load-displacement curves and the distribution of the equivalent stress of this type of sheet forming process (stretching forming) show the feasibility of all proposed models, highlighting however the main advantage of the Multi-Mechanisms and of the Polycrystalline models as compared to the classical unified Hill formalism using constant values of Hill parameters. In a future will be make more comparisons with experimental results using channel die compression, biaxial tensile and simple shear tests in order to obtain a complete description of tridimensional plastic anisotropy corresponding to large deformations. Moreover a lot of experimental and numerical analysis of a deep drawing process applied to a thick sheet will be considered.

References

[1] Banabic D., Bunge H.-J., Pohlandt K., Tekkaya A.E.: Formability of metallic materials, Springer-Verlag, Berlin–Heidelberg–New York, 2000.

[2] Seidt, J.D., Plastic Deformation and Ductile Fracture of 2024-T351 Aluminum under Various Loading Conditions, Ph.D. Thesis, Graduate School of the Ohio State University, 2010.

[3] Hill, E., A theory of the yielding and plastic flow of anisotropic metals, Proc. Roy. Soc., London, 1948.

[4] Zhang, S., Francillette, H., Gavrus, A., Analysis of the anisotropic behavior and the formability aptitude for an AA2024 alloy using channel die compression test and the simple tension test, Key Eng. Mat., 504-506, pp.23-28, 2012.

[5] Cailletaud, G., Saï, K., A polycrystalline model for the description of ratchetting: Effect of intergranular and intragranular hardening, Mat. Sci. Eng., 480, pp. 24-39, 2008.

[6] Saï, K., Multi-mechanism models: Present state and future trends, Int. J. Plast, 27, pp. 250-281, 2011.

[7] Nasri, W., Gavrus, A., Kouadri, A., Saï, K., Applications of multi-scale models to numerical simulation and experimental analysis of anisotropic elastoplastic behavior of metallic sheets, Key Eng. Mat., 611-612, pp. 536-544, 2014.

[8] W. Hosford, Mechanical Behavior of Materials, Cambridge University Press, New York, 2005.

[9] J. Besson, R. Leriche, R. Foerch, G. Cailletaud, Rev. Eur. Elem. Finis 7 (1998) 567–588

[10] Voce, E., A practical strain hardening function, Metallurgia, 51 (307), pp. 219-226, 1955.